Supporting Information

Exceptional Alkaline Hydrogen Evolution by Molybdenum-Oxide-Nitride-based Electrocatalysts with Fast Water-Dissociation and Hydrogen-Adsorption Kinetics

Zhongmin Wang,*[a] Jing Qu,[a,b] Yanxiang He,[c] Tuzhi Xiong,[c] Zhimin Huang,[a] Feng Wang,*[b] M.-Sadeeq Balogun*[b,c]

XPS experimental parameters

X-ray photoelectron spectroscopy (XPS) analysis was performed using The ESCA lab 250 test. The instrument used a monochromated Al Kα source 1486.6 eV and the base pressure was 5 × 10−10 Torr. The sample area analyzed was about 700 μm × 300 μm. A pass energy (PE) of 80 eV, corresponding to an all over Fermi edge resolution of 0.89 ± 0.02 eV with a 0.5 eV step, was used to acquire wide range survey spectra. A PE of 20 eV, corresponding to an all over Fermi edge resolution of 0.39 ± 0.02 eV with a 0.1 eV step, was used to acquire narrow spectra of the Mo 3d, C 1s, O 1s, Ni 2p, and N 1s orbitals. A PE of 40 eV, corresponding to an all over Fermi Edge resolution of 0.56 ± 0.02 eV with a 0.15 eV step, was used to acquire spectra at the valence band energy region. All data were acquired using charge compensation to establish a steady state surface potential.

XPS data including peak fitting, line shape synthesis, envelope background modeling and subtraction was processed using the XPSpeak41. The acquired spectra required a binding energy calibration based on identifying a component peak within a data envelope. The procedure adopted was based on aligning a component peak within the O 1s spectrum rather than the more usual alignment based on a component within the C 1s spectrum. For the fitting of the Mo 3d XPS spectra, $d_5:d_3$ = 3:2. For the fitting of the Ni 2p XPS spectra, $p_3:p_1$= 2:1.

For the peak area, the fitting of the Mo 3d XPS spectra was d5:d3 = 3:2 and Ni 2p XPS spectra was p3:p1= 2:1.

The FWHM of all the Mo 3d peaks for $NiMoO_4/MoO_2$ include 2.33, 1.19, 1.83 and 1.89 for Mo^{4+} $3d_{5/2}$, Mo^{6+} $3d_{5/2}$, Mo^{4+} $3d_{3/2}$ and Mo^{6+} $3d_{3/2}$, respectively. The FWHM of the Ni 2p peaks for $NiMoO_4/MoO_2$ include 2.21, 3.61, 3.42, 2.21, 2.69 and 4.27 for Ni^{2+} $2p_{3/2}$, Ni^{3+} $2p_{3/2}$, Ni^{sat} $2p_{3/2}$, Ni^{2+} $2p_{1/2}$, Ni^{3+} $2p_{1/2}$ and Ni^{sat} $2p_{1/2}$, respectively. The FWHM of the O 1s peaks for $NiMoO_4/MoO_2$ include 1.52, 1.58 and 2.12 for Mo-O of MoO_2, Mo-O of $NiMoO_4$ and adsorbed water molecules (O_w) and Ni^{sat} $2p_{1/2}$, respectively.

The FWHM of all the Mo 3d peaks for $Ni_{0.2}Mo_{0.8}N/MoO_2$ include 1.15, 1.44, 1.59, 0.96, 1.47 and 1.25 for Mo^{3+} $3d_{5/2}$, Mo^{4+} $3d_{5/2}$, Mo^{3+} $3d_{3/2}$, Mo^{6+} $3d_{5/2}$, Mo^{4+} $3d_{3/2}$ and Mo^{6+} $3d_{3/2}$, respectively. The FWHM of all the Ni 2p peaks for $Ni_{0.2}Mo_{0.8}N/MoO_2$ include 1.47, 2.30, 3.00, 2.75, 2.69, 2.37, 3.32 and 3.31 for Ni^0 $2p_{3/2}$, Ni^{2+} $2p_{3/2}$, Ni^{3+} $2p_{3/2}$, Ni^{sat} $2p_{3/2}$, Ni^0 $2p_{1/2}$, Ni^{2+} $2p_{1/2}$, Ni^{3+} $2p_{1/2}$ and Ni^{sat} $2p_{1/2}$, respectively. The FWHM of the O 1s peaks for $Ni_{0.2}Mo_{0.8}N/MoO_2$ include 1.79 and 3.05 for Mo-O of MoO_2, Mo-O and oxygen deficient (O_d) and Ni^{sat} $2p_{1/2}$, respectively.

ECSA Calculation

The C_{dl} was calculated according to the following equation:

$$C_{dl} = |ja - jc|/2 \, ,$$

where j_a and j_c are charging and discharging current densities and υ is the scan rate. [1] The potential range of the measurements is from −0.93 to −0.82 V vs. SCE in a non-Faradaic region for the HER and the scan rates were from 1.0 to 8.0 mV s^{-1}. The difference of charging and discharging current densities at 0.01 V vs. RHE was used for calculation.

Conversion of C_{dl} to ECSA

The specific capacitance for a flat surface is generally found to be in the range of 20 - 60 μF cm^{-2}. In the following calculations of ECSA, we assume specific capacitance as 40 μF cm^{-2}.

$$ECSA = \frac{Cdl}{40 \, \mu F \, cm - 2} \qquad (2)$$
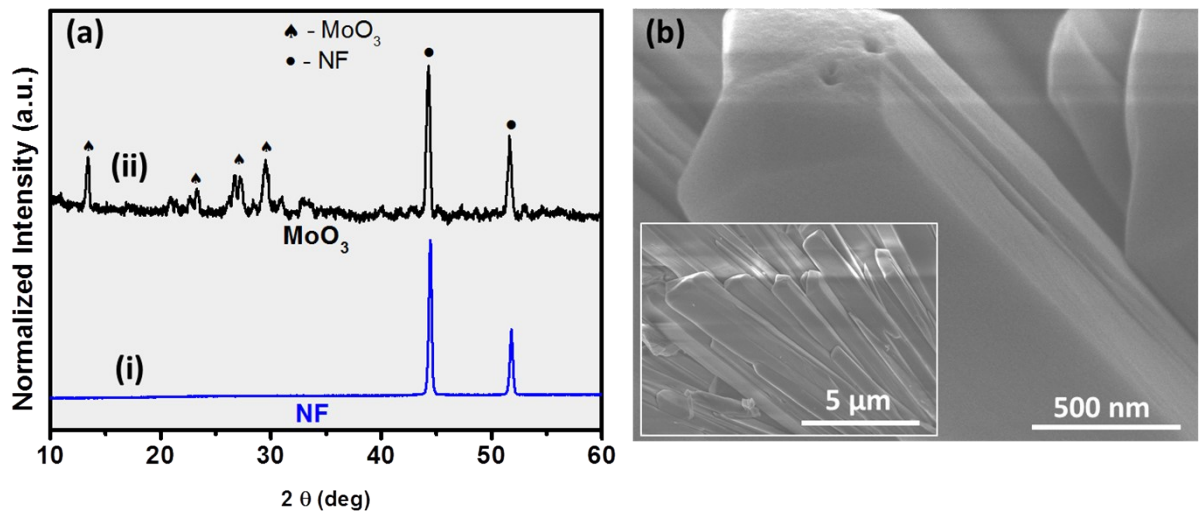
Figure S1. (a) XRD of the NF and MoO$_3$ precursor. (b) SEM images of the MoO$_3$ precursor.
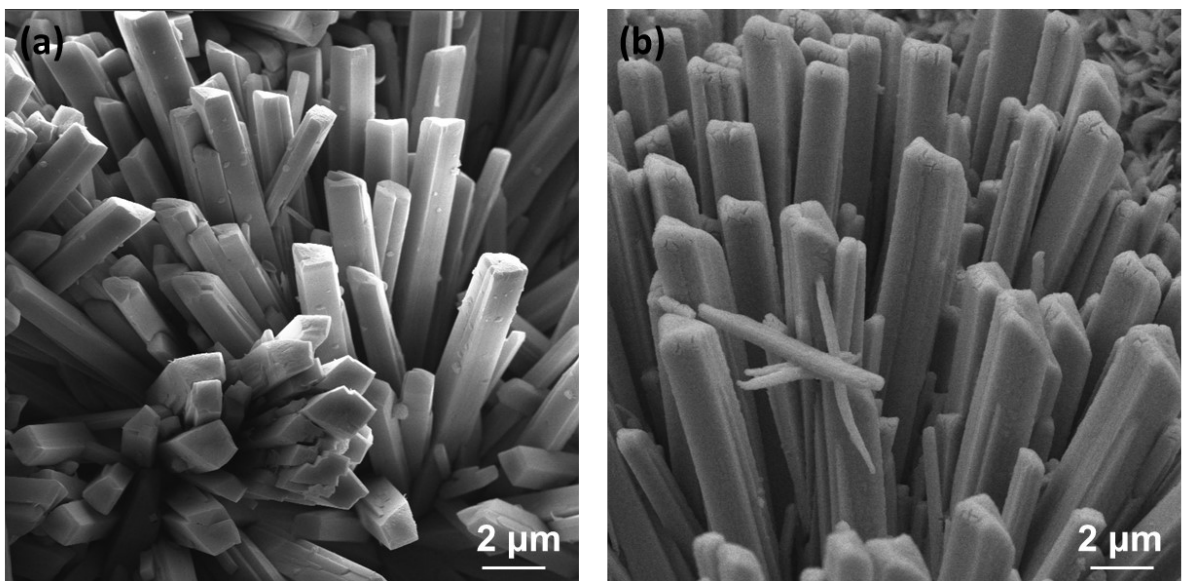
Figure S2. Low magnification SEM images of the (a) NiMoO$_4$/MoO$_2$ and (b) Ni$_{0.2}$Mo$_{0.8}$N/MoO$_2$.
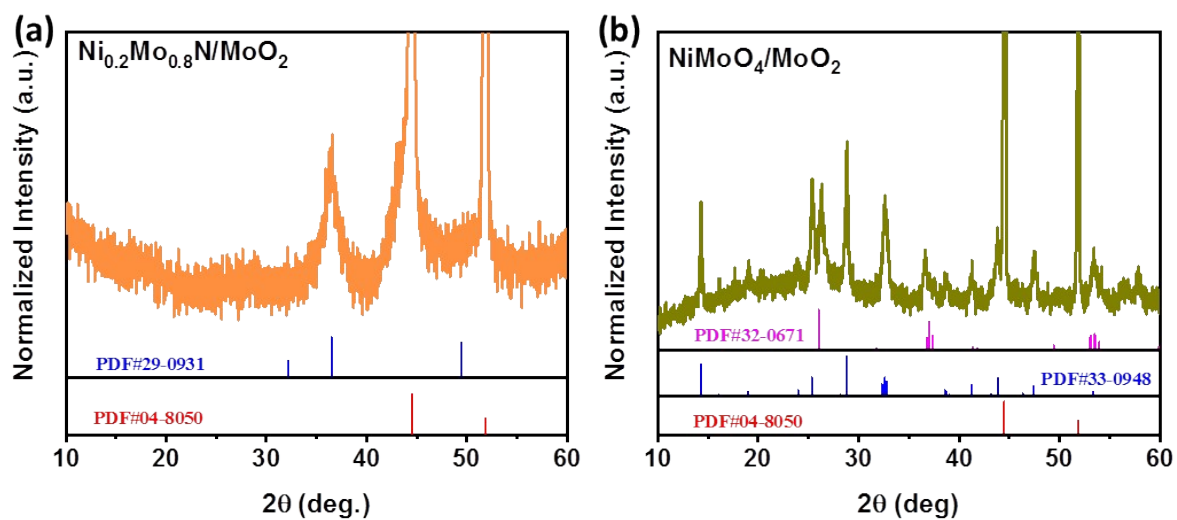
Figure S3. (a) XRD spectra of the $Ni_{0.2}Mo_{0.8}N/MoO_2$ and $NiMoO_4/MoO_2$ samples in the powdered form. XRD spectra of the (b) $Ni_{0.2}Mo_{0.8}N/MoO_2$ and (c) $NiMoO_4/MoO_2$ samples on the NF.
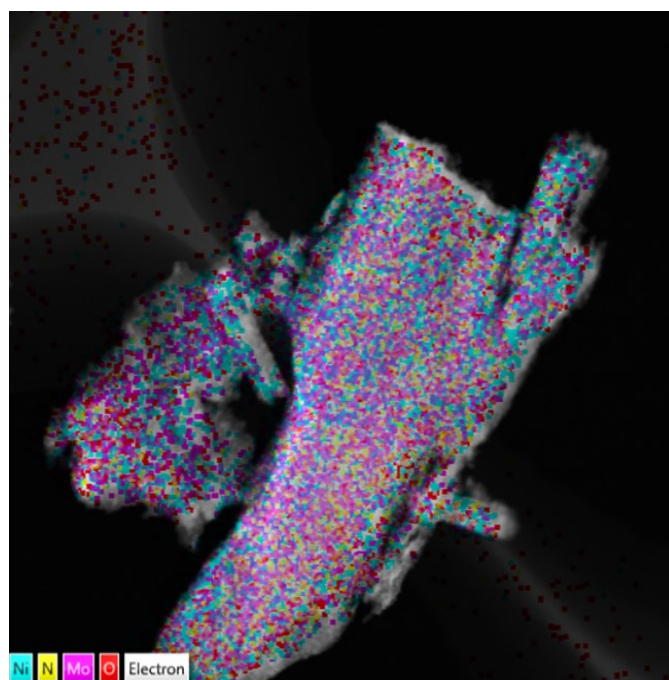
Figure S4. Sum of the elemental mapping image of the $Ni_{0.2}Mo_{0.8}N/MoO_2$ nanorods.

Table S1. Quantitative information from the EDS/EDX to complement the mapping images of the $Ni_{0.2}Mo_{0.8}N/MoO_2$ sample.

Elements	Atomic %
N	8.76
O	35.99
Ni	21.02
Mo	34.23
Total:	100.00
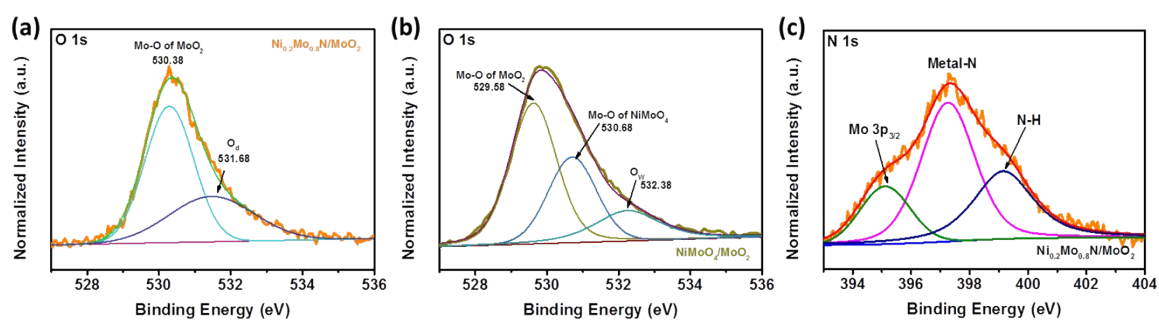
Figure S5. O 1s XPS spectra of (a) $Ni_{0.2}Mo_{0.8}N/MoO_2$ and (b) $NiMoO_4/MoO_2$. (c) N 1s XPS spectra of $Ni_{0.2}Mo_{0.8}N/MoO_2$.

Table S2. HER properties of recently reported NiMoN-based catalysts.

Catalyst	HER, η @ 10 mA cm^{-2}	Tafel slope, mV dec^{-1}	Reference
$Ni_{0.2}Mo_{0.8}N/MoO_2$	13	264	This work
$NiMoO_4/MoO_2$	194	323	This work
$Ni_3N/Ni_{0.2}Mo_{0.8}N/NF$	55	246	[2]
$Ni_{0.2}Mo_{0.8}N/Fe–Ni_3N/NF$	40@20	266	[3]
hexagonal V-$Ni_{0.2}Mo_{0.8}N$	39	245@25	[4]
$Ni_{0.2}Mo_{0.8}N/NiMoP_2/MoO_2@NC$	48	-	[5]
$Ni_{0.2}Mo_{0.8}N/Ni$ heterostructures	14	-	[6]
$Ni_{0.2}Mo_{0.8}N/Ni_3N$	49	-	[7]
$NiSe_2–NPs/NiMoN–NRs$	58	241	[8]
Ni_3N-Mo_2N/NF	66	252	[9]
$Ni_3N-NiMoN$	31	277	[10]
$Ni-Fe/NiMoN_x$	49@20	260@20	[11]

Table S3. The relevant parameters from the fitted the Nyquist plots of the catalysts in HER.

Electrodes	R_s (Ω)	R_{ct} (Ω)
$NiMoO_4/MoO_2$	1.93	3.17
$Ni_{0.2}Mo_{0.8}N/MoO_2$	2.33	1.58
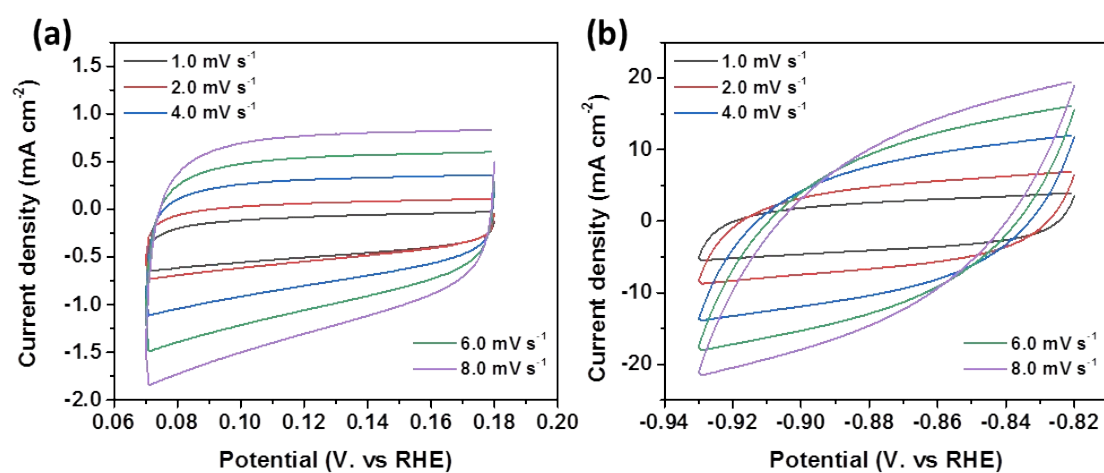
Figure S6. CV curves of (a) $NiMoO_4/MoO_2$ and (b) $Ni_{0.2}Mo_{0.8}N/MoO_2$ for the HER.
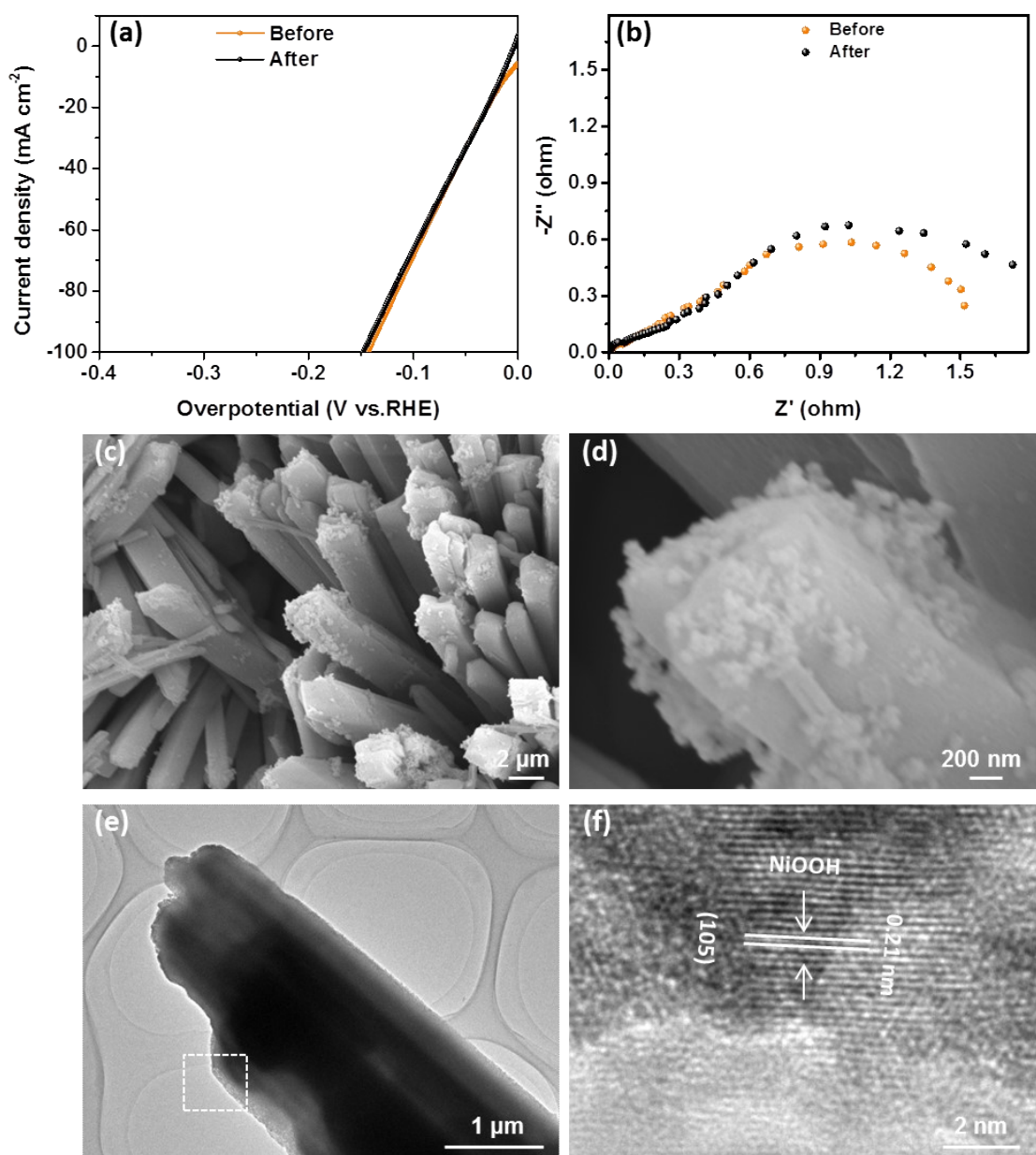
Figure S7. (a) HER polarization curves and (b) Nyquist plots of the $Ni_{0.2}Mo_{0.8}N/MoO_2$ catalyst

after stability test. (c, d) SEM and (e, f) TEM images of $Ni_{0.2}Mo_{0.8}N/MoO_2$ after stability test.
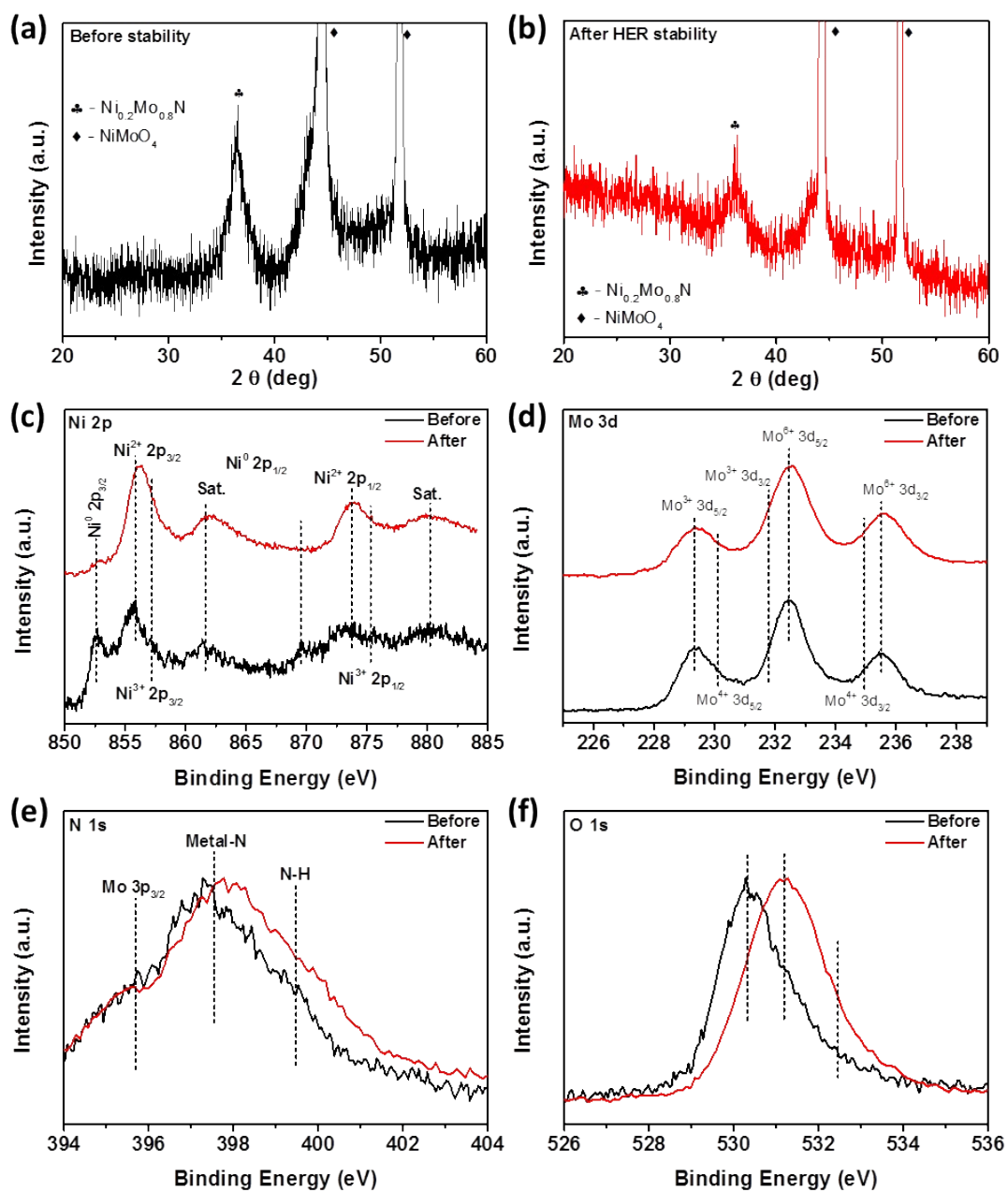
Figure S8. XRD spectra of $Ni_{0.2}Mo_{0.8}N/MoO_2$ (a) before and (b) after HER stability test. (c) Ni 2p, and (d) Mo 3d, (e) N 1s and (f) O 1s XPS spectra of $Ni_{0.2}Mo_{0.8}N/MoO_2$ before and after HER stability test.
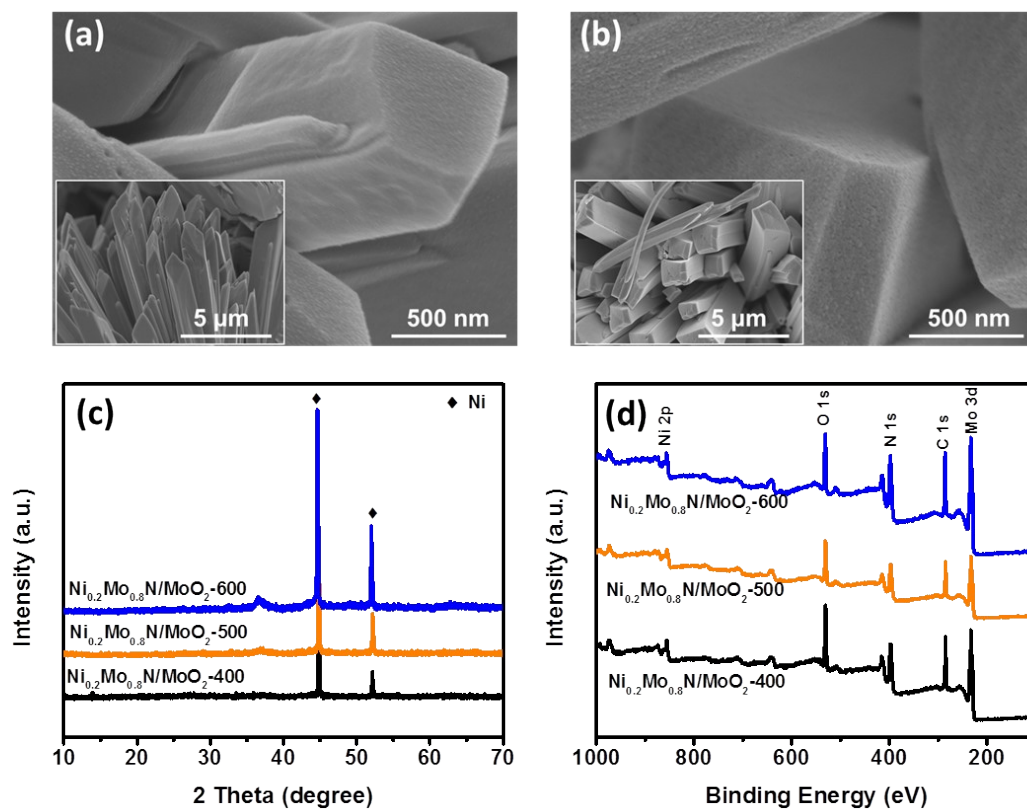
Figure S9. SEM images of (a) $Ni_{0.2}Mo_{0.8}N/MoO_2$-400 and (b) $Ni_{0.2}Mo_{0.8}N/MoO_2$-600. (c) XRD pattern and (d) XPS survey spectra of $Ni_{0.2}Mo_{0.8}N/MoO_2$-400, $Ni_{0.2}Mo_{0.8}N/MoO_2$-500 (optimized catalyst) and $Ni_{0.2}Mo_{0.8}N/MoO_2$-600.
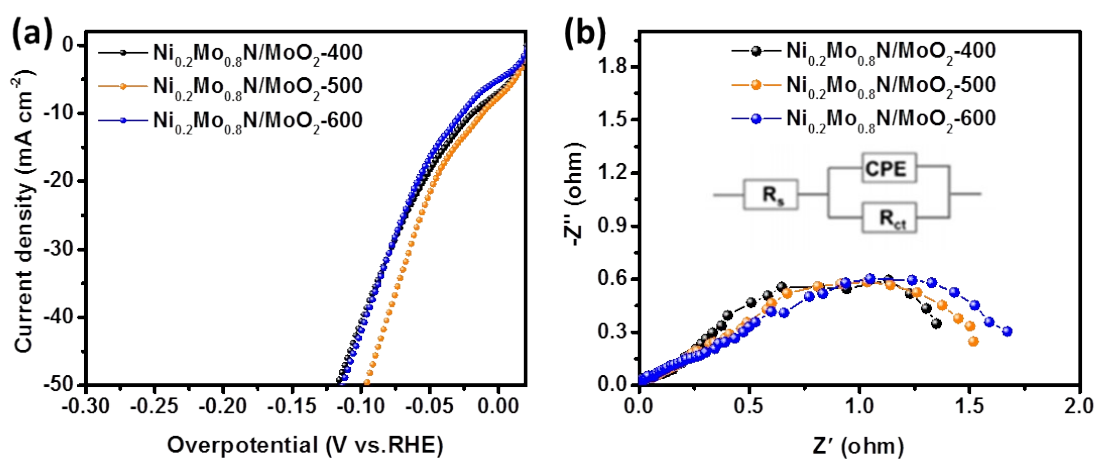
Figure S10. (a) HER Polarization curves and (b) Nyquist plots of $Ni_{0.2}Mo_{0.8}N/MoO_2$-400, $Ni_{0.2}Mo_{0.8}N/MoO_2$-500 (optimized catalyst) and $Ni_{0.2}Mo_{0.8}N/MoO_2$-600.

Table S4. The relevant parameters from the fitted the Nyquist plots of the catalysts in HER.

Electrodes	R_s (Ω)	R_{ct} (Ω)
$Ni_{0.2}Mo_{0.8}N/MoO_2$-400	2.06	1.96
$Ni_{0.2}Mo_{0.8}N/MoO_2$-500	2.33	1.58
$Ni_{0.2}Mo_{0.8}N/MoO_2$-600	1.68	1.89
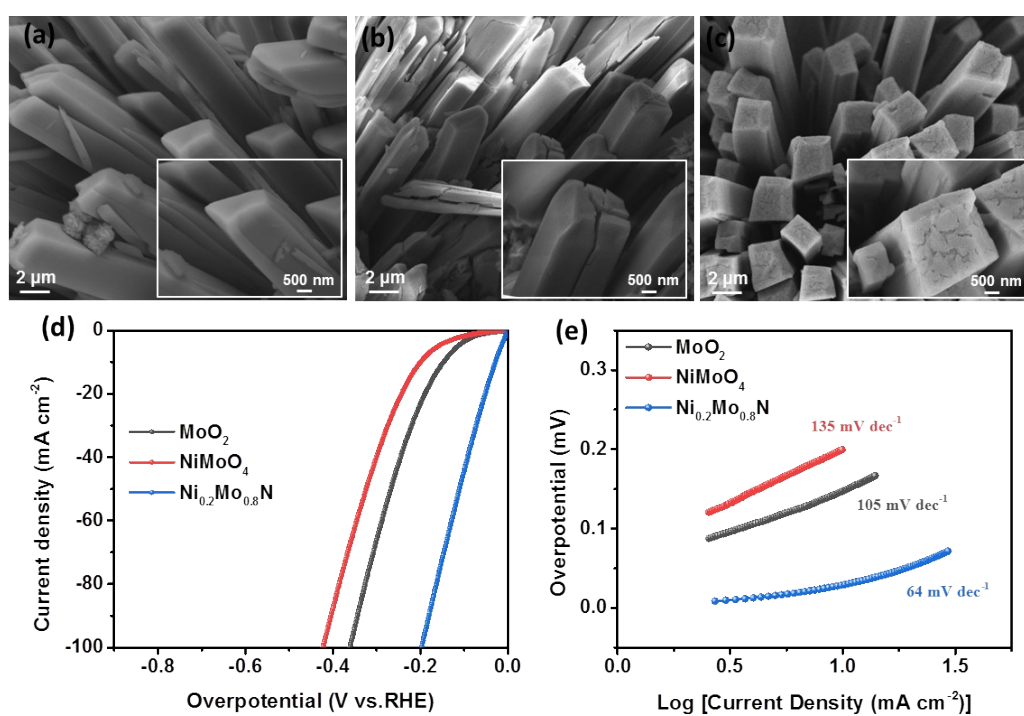
Figure S11. SEM images of (a) $NiMoO_4$, (b) MoO_2 and (c) $Ni_{0.2}Mo_{0.8}N$. (d) LSV curves and (e) Tafel plots of $NiMoO_4$, MoO_2 and $Ni_{0.2}Mo_{0.8}N$ for the HER.
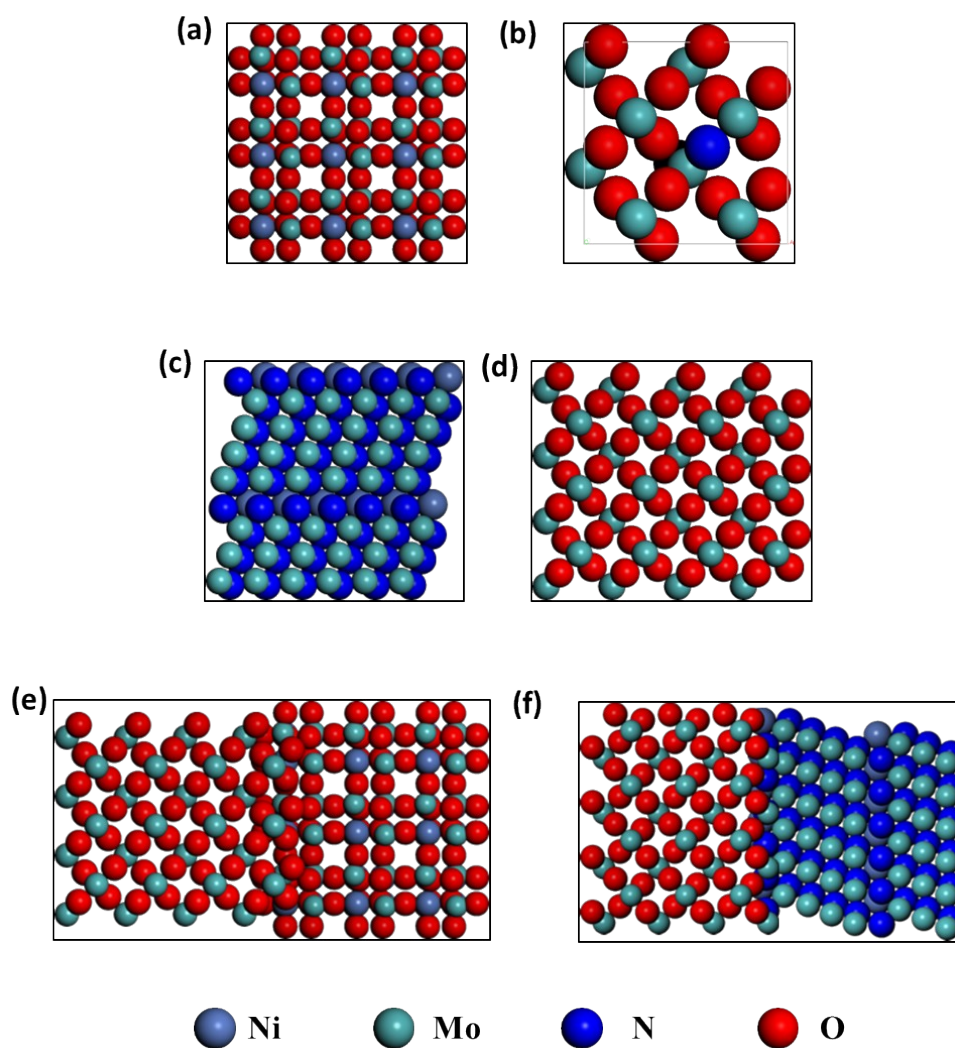
Figure S12. The structural models of (a)MoO$_2$, (b) N-MoO$_2$, (c) Ni$_{0.2}$Mo$_{0.8}$N, (d) NiMoO$_4$, (e) NiMoO$_4$/MoO$_2$ and (f) Ni$_{0.2}$Mo$_{0.8}$N/MoO$_2$.
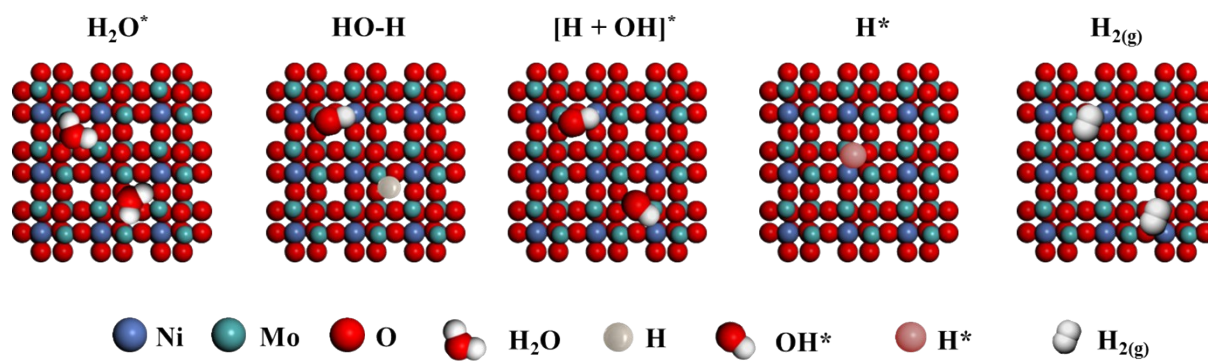
Figure S13. The optimized structural models for the water adsorption, water activation, water dissociation, hydrogen adsorption and hydrogen evolution on MoO$_2$.
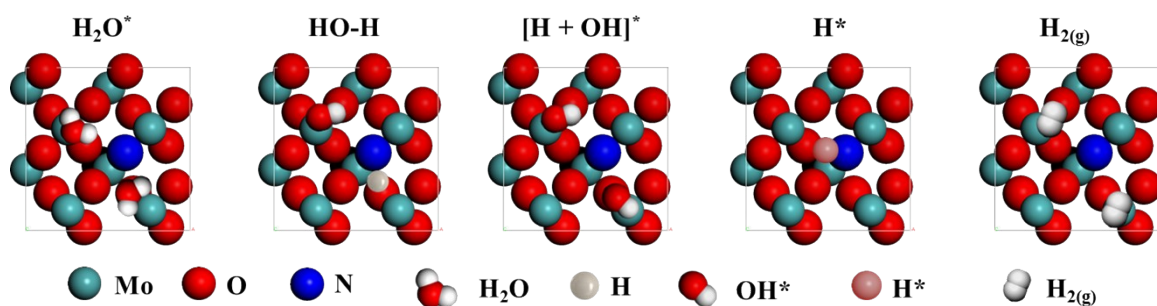
Figure S14. The optimized structural models for the water adsorption, water activation, water dissociation, hydrogen adsorption and hydrogen evolution on N-MoO$_2$.
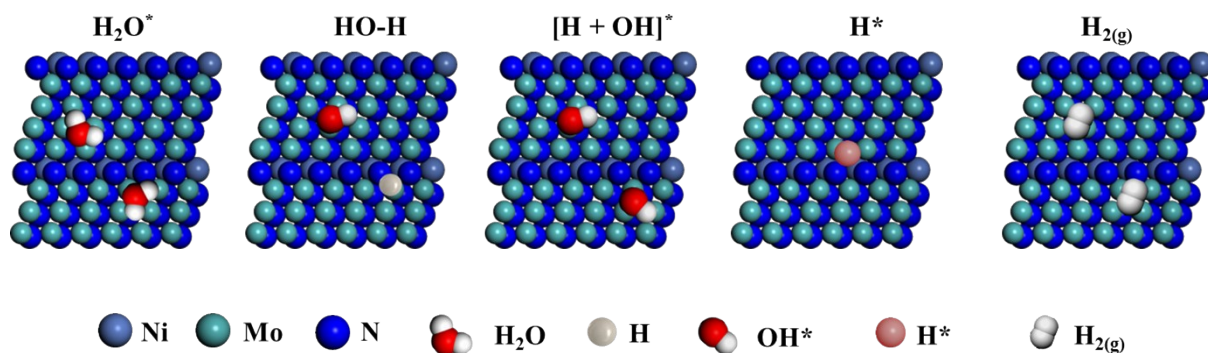
Figure S15. The optimized structural models for the water adsorption, water activation, water dissociation, hydrogen adsorption and hydrogen evolution on Ni$_{0.2}$Mo$_{0.8}$N.
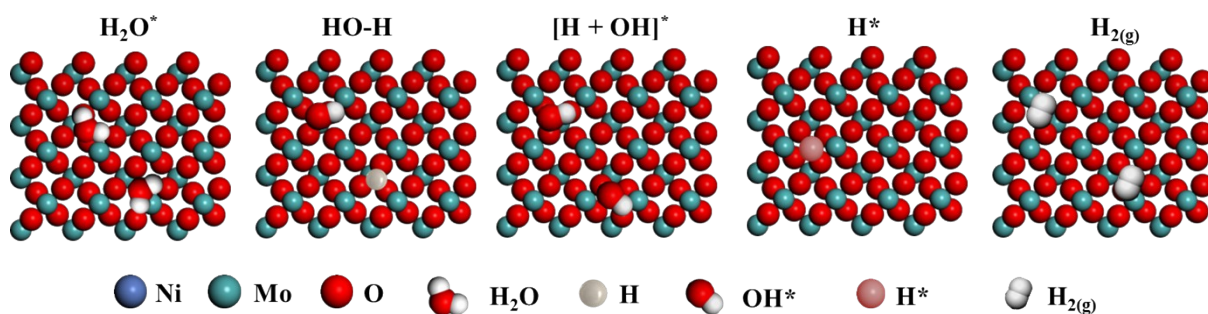
Figure S16. The optimized structural models for the water adsorption, water activation, water dissociation, hydrogen adsorption and hydrogen evolution on NiMoO$_4$.
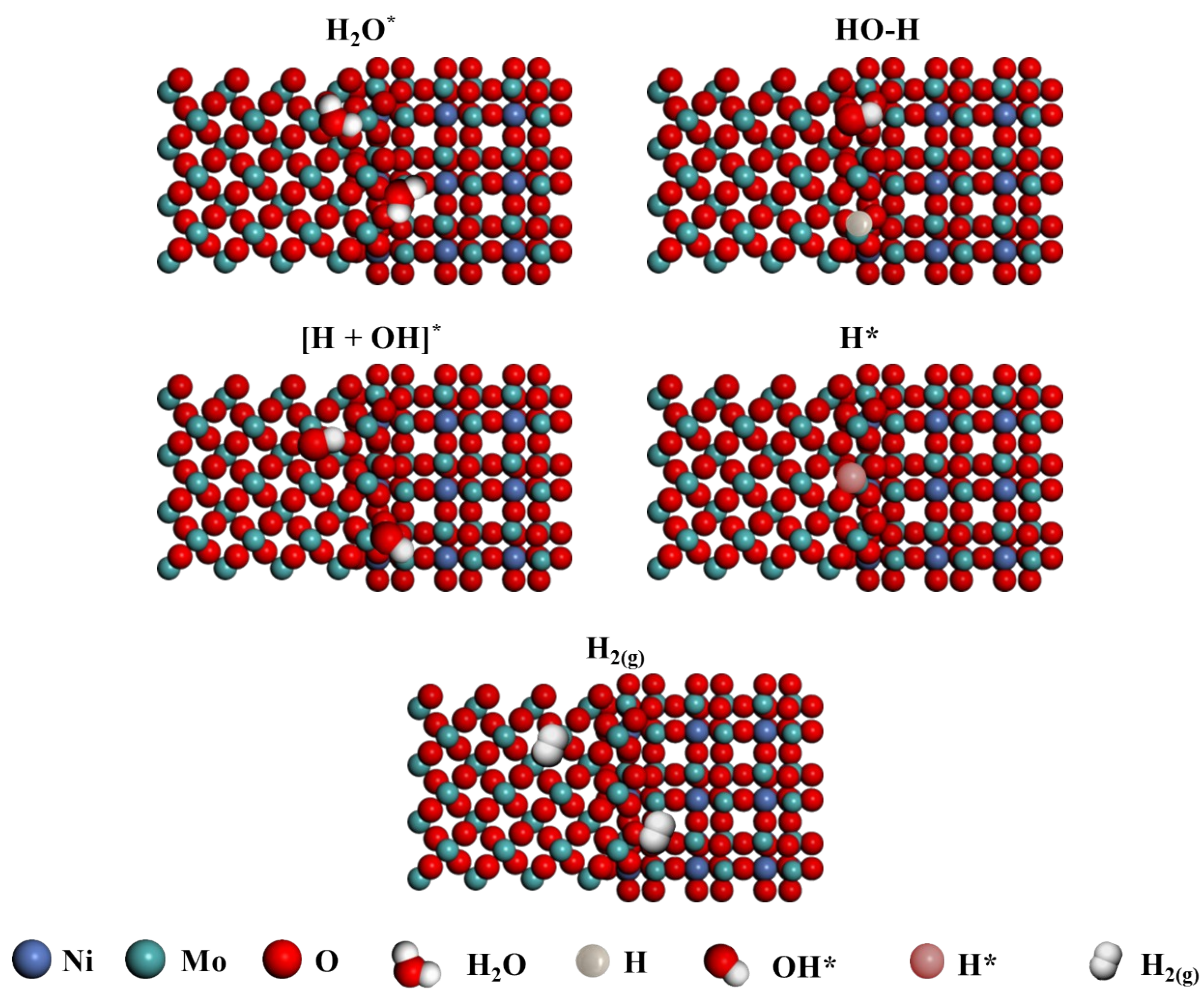
Figure S17. The optimized structural models for the water adsorption, water activation, water dissociation, hydrogen adsorption and hydrogen evolution on $NiMoO_4/MoO_2$.
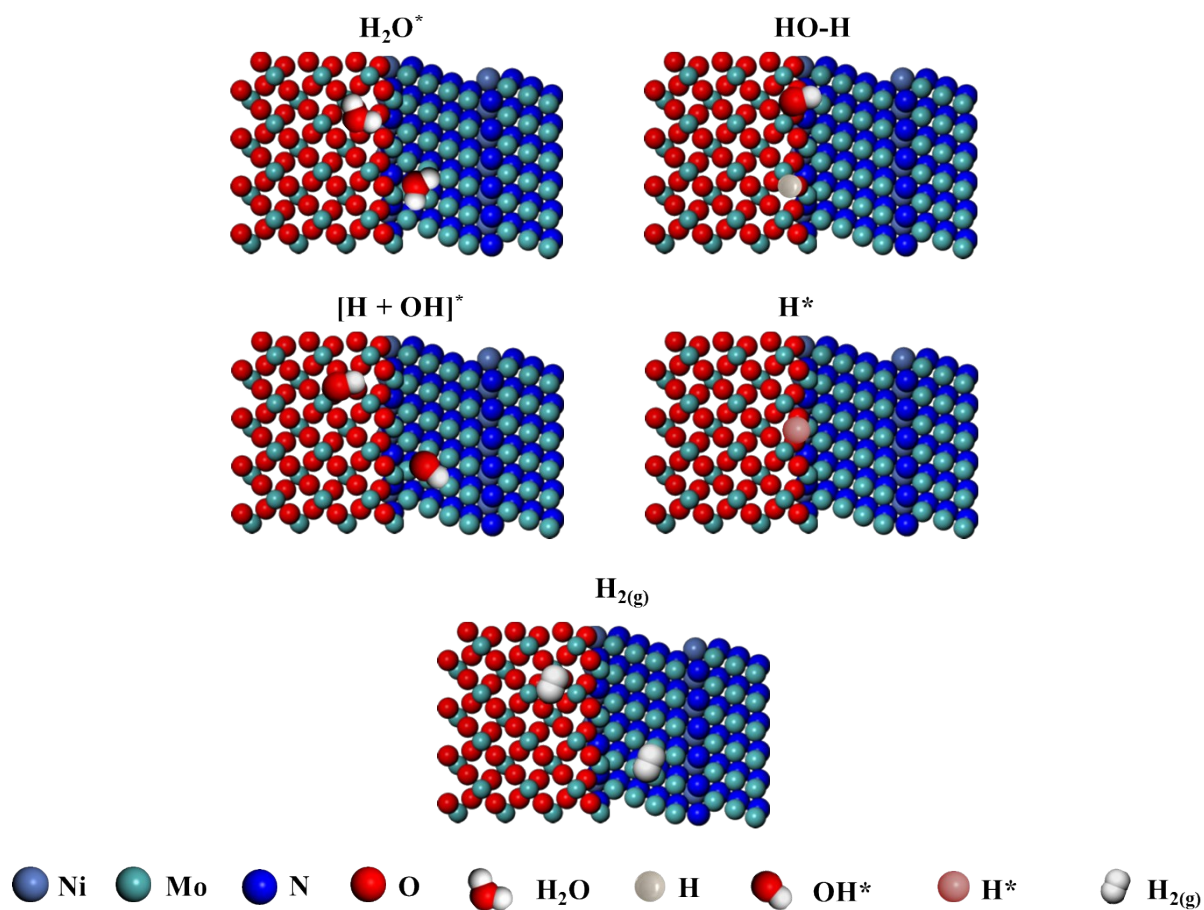
Figure S18. The optimized structural models for the water adsorption, water activation, water dissociation, hydrogen adsorption and hydrogen evolution on $Ni_{0.2}Mo_{0.8}N/MoO_2$.
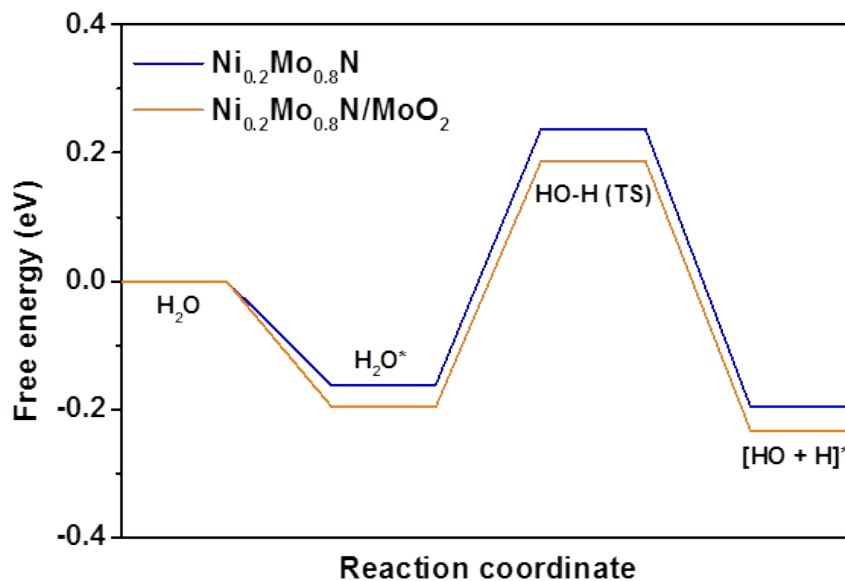
Figure S19. The HER free-energy diagram of H_2O adsorption, activation and dissociation on $Ni_{0.2}Mo_{0.8}N$ and $Ni_{0.2}Mo_{0.8}N/MoO_2$ model catalysts.

References

1.   K. Xu, Y. Sun, X. Li, Z. Zhao, Y. Zhang, C. Li and H. J. Fan, *ACS Mater. Lett.*, 2020, **2**, 736-743.

2.   R.-Q. Li, X.-Y. Wan, B.-L. Chen, R.-Y. Cao, Q.-H. Ji, J. Deng, K.-G. Qu, X.-B. Wang and Y.-C. Zhu, *Chem. Eng. J.*, 2021, **409**, 128240.

3.   C. Liu, H. Zhu, S. Lu, F. Xu, F. Duan and M. Du, *RSC Adv.*, 2021, **11**, 19797-19804.

4.   P. Zhou, X. Lv, D. Xing, F. Ma, Y. Liu, Z. Wang, P. Wang, Z. Zheng, Y. Dai and B. Huang, *Appl. Catal. B-Environ.*, 2020, **263**, 118330.

5.   Y. Yan, X. Cao, L. Ning, F. Lin, W. Qin, X. Liu and W. Gu, *ACS Appl. Nano Mater.*, 2022, **5**, 7778-7786.

6.   B. Zhang, L. Zhang, Q. Tan, J. Wang, J. Liu, H. Wan, L. Miao and J. Jiang, *Energy Environ. Sci.*, 2020, **13**, 3007-3013.

7.   B. Wang, L. Guo, J. Zhang, Y. Qiao, M. He, Q. Jiang, Y. Zhao, X. Shi and F. Zhang, *Small*, 2022, **18**, 2201927.

8.   J. Wang, D. T. Tran, K. Chang, S. Prabhakaran, D. H. Kim, N. H. Kim and J. H. Lee, *Energy Environ. Mater.*, 2022, **DOI:** 10.1002/eem2.12526.

9.   R. Dai, H. Zhang, W. Zhou, Y. Zhou, Z. Ni, J. Chen, S. Zhao, Y. Zhao, F. Yu, A. Chen, R. Wang and T. Sun, *J. Alloy. Compd.*, 2022, **919**, 165862.

10.   A. Wu, Y. Xie, H. Ma, C. Tian, Y. Gu, H. Yan, X. Zhang, G. Yang and H. Fu, *Nano Energy*, 2018, **44**, 353-363.

11.   Y. Qiu, M. Sun, J. Cheng, J. Sun, D. Sun and L. Zhang, *Catal. Commun.*, 2022, **164**, 106426.